NATIONAL ADVISORY COMMITTEE FOR AERONAUTICS

TECHNICAL MEMORANDUM

No. 1209

EXPERIMENTAL STUDY OF FLOW PAST TURBINE BLADES

By E. Eckert and K. v. Vietinghoff-Scheel

Translation of "Versuche über die Strömung durch Turbinenschaufelgitter"
Vorabdrucke aus Jahrbuch 1942 der deutschen
Luftfahrtforschung, 6. Lieferung

NACA

Washington

June 1949

NATIONAL ADVISORY COMMITTEE FOR AERONAUTICS

TECHNICAL MEMORANDUM NO. 1209

EXPERIMENTAL STUDY OF FLOW PAST TURBINE BLADES[*]

By E. Eckert and K. v. Vietinghoff-Scheel

OUTLINE

I. INTRODUCTION

The requirements on gas turbines for aircraft power units, namely, adequate efficiency, operation at high gas temperatures, low weight, and small dimensions, must be taken into consideration during the design of the blading. To secure good efficiency, it is necessary that the gas flow past the blades as smoothly as possible without separation. This is relatively easily obtainable in the accelerated flow of turbine blading, if the blade spacing is chosen small enough. A small blade spacing, however, is detrimental to the other requirements outlined above. Operation at high gas temperatures usually calls for blade cooling. This cooling is associated with a power input that lowers the turbine efficiency. Since the amount of heat that must be carried off for cooling a blade can be influenced rather little, the gross power input for a turbine stage can be reduced by keeping the number of blades to a minimum, that is, with blades of high spacing ratio. But here also a limit is imposed, the exceeding of which is followed by separation of flow. Hence the requirement of finding blade forms on which the flow separates at rather high spacing ratios.

Small dimensions of the turbine are essentially obtained by keeping the outside diameter of the blading as small as possible. This is made possible by choosing a high tip speed and making the width of the annular space of the turbine stage available for the passage of the gas great, that is, the inside diameter as small as possible. But on such long blades the flow at the inside diameter is appreciably different from that at the outside diameter. The flow strikes the rotor blades inside at a

_____

much flatter angle than outside. The turbine blades must therefore ensure
a flow free from separation throughout the whole available range of flow
angles.

Since the visualization of the separation phenomena on a running
turbine involves considerable difficulties, it is appropriate to study
the flow first on blade grids at rest. Direct application of such
findings to the guide vanes of a turbine is probably possible. Greater
care is advised in application to rotor blades. On these the boundary
layer, which forms at the surface of the blades, is under the influence
of the centrifugal force. This should not affect the separation phenomena
on axial turbines very much, where the centrifugal force is perpendicular
to the direction of motion. A greater effect is to be expected on radial
turbines, where the centrifugal force acts against the separation when
the gas flows through the turbine from the inside toward the outside. In
the reversed flow direction the centrifugal-force effects favor separation
of flow.

The use of the interference method for the study of flow past the
blade grids (references 1 and 2) has the advantage that the tests can be
run at Reynolds and Mach numbers encountered on actual turbines. On top
of that, interference photographs not only afford a qualitative picture
of the flow process, but also can be interpreted quantitatively, such as
the determination of the pressure distribution over the blades and with
it the torque exerted on the rotor, for instance.

II. ESTIMATION OF PRESSURE DISTRIBUTION OVER TURBINE BLADES

To the torque exerted by the flowing gas on the rotor there corre-
sponds a force on each blade in circumferential direction. This force
is introduced by low pressure at the back of the blade and by high pres-
sure at the face of the blade, in the same manner as the lift on an air-
foil. Weinig (reference 3) computed the pressure distribution caused
by the flow of a frictionless fluid for several blade forms, one of which
is represented in figure 1, by the pressure distribution curve for a

blade grid with spacing ratio $\frac{a}{t} = 0.96$ and flow direction w_1. The

viscosity of the flowing gas causes a boundary layer along the blade
surface, and it is this, as is known, that effects the separation at
the blade as soon as the pressure rise in flow direction along the blade
surface exceeds a certain value. To be feared most of all is a sepa-
ration at the back in the area between A and B, although it can occur
equally on the face at C. The amount of pressure rise which a boundary
layer can overcome without separation depends upon whether the layer is
laminar or turbulent. It is therefore to be expected that the separation
phenomena discussed hereinafter are affected by the Reynolds number.

The order of magnitude of the pressure rise to be overcome by the
flow past a turbine blade is readily estimated when the entrance and exit

angle of flow for the blading are known. Weinig's calculations (fig. 1) as well as the test data on wings and cascades of airfoils (references 4 and 5) give the pressure distribution curve an approximately triangular form. Giving the pressure distribution projected on a straight line (width of grid b in fig. 2) perpendicular to the grid direction the shape of a triangle as represented in figure 3, the magnitude of the force U per unit blade length exerted by the flow in grid direction is

$$U = \frac{\Delta p_m b}{2} \qquad (1)$$

where Δp_m is the maximum pressure difference between front and back of blade, and b the width of the blade grid. On the other hand, by the momentum theorem with the notation of figure 2A this force U follows the equation

$$U = \rho a w_m \left(w_{u2} - w_{u1} \right) \qquad (2)$$

the flow velocities being assumed so small that constant gas density ρ can be assumed. Since an estimate is involved, this is possible up to the speed of about two thirds the velocity of sound. This assumption simplifies the calculation, which, of course, can be carried out for variable density just as well. The velocity components w_u are introduced vectorially in equation (2), that is, subtracted when in the same direction, but added when directed oppositely. Determining the maximum pressure difference from equations (1) and (2) gives

$$\Delta p_m = 2\rho \frac{a}{b} w_m \left(w_{u2} - w_{u1} \right) \qquad (3)$$

The stage pressure drop Δp_{st} is the difference of the static pressures p_1 and p_2 upstream and downstream from the blade grid as

$$\Delta p_{st} = p_1 - p_2 = \frac{\rho}{2} \left(w_2{}^2 - w_1{}^2 \right) = \frac{\rho}{2} \left(w_{u2}{}^2 - w_{u1}{}^2 \right) \qquad (4)$$

The dynamic pressure of the flow velocity is

$$q_1 = \frac{\rho}{2} w_1{}^2 \qquad (5)$$

With these quantities the pressure distribution triangle can be plotted to scale, as exemplified in figure 3A, because the pressure at the blade

trailing edge, that is, at the tip of the triangle, is practically p_2. The amount of the pressure rise at the back of the blade follows then as the difference between p_2 and the lowest pressure p_3 as

$$p_2 - p_3 = \Delta p_m - q_1 - \Delta p_{st} \tag{6}$$

Whether the boundary layer is able to overcome this pressure rise without separation depends upon the magnitude of the kinetic flow energy relative to this pressure rise. The velocity increases from w_1 to w_2 during the flow through the blade grid. For the present estimate, therefore, it is best and perhaps accurate enough as well to refer the pressure rise $p_2 - p_3$ to the average kinetic energy of flow

$$q = \frac{1}{2}\left(\frac{\rho w_1^2}{2} + \frac{\rho w_2^2}{2}\right) \tag{7}$$

With equation (6) we then get

$$\frac{p_2 - p_3}{q} = 8\frac{a}{b}\frac{w_m\left(w_{u2} - w_{u1}\right)}{w_1^2 + w_2^2} - \frac{2w_1^2}{w_1^2 + w_2^2} - 2\frac{w_{u2}^2 - w_{u1}^2}{w_1^2 + w_2^2} \tag{8}$$

as measure for the danger of separation.

The pressure distribution triangle in figure 3A relates to a turbine stage with axial entry $\left(w_{u1} = 0\right)$ and an exit angle β_2 of 20° $\left(w_m/w_{u2} = \tan\beta_2 = 0.364\right)$ measured against the circumferential direction.

Reversing the flow through the blade grid involves a pressure rise from p_2 toward p_1. The blades must then, of course, be shaped a little differently, the pointed tip of the blade being placed on the exit side again, as exemplified in figure 2B. Equations (3), (4), and (7) remain valid for this direction of flow. But the dynamic pressure of the flow velocity is

$$q_2 = \frac{\rho}{2}w_2^2 \tag{9}$$

The pressure distribution triangle assumes the form represented in figure 3B, and the referred pressure rise at the blade back amounts to

$$\frac{p_2 - p_3}{q} = 8 \frac{a}{b} \frac{w_m\left(w_{u2} - w_{u1}\right)}{w_2^2 + w_1^2} - \frac{2w_2^2}{w_1^2 + w_2^2} + 2 \frac{w_{u2}^2 - w_{u1}^2}{w_1^2 + w_2^2} \qquad (10)^*$$

The flow directions of figure 3B are the same as in figure 3A. A comparison of these two triangles indicates that the pressure rise, referred to the average kinetic energy of flow which the boundary layer has to overcome, is substantially higher for the blower blade than for the turbine blade. This is the reason such marked deflection as assumed in figure 3 can apparently not be achieved at all in a blower blading without separation. According to equations (8) and (10) the danger of separation is so much greater as the flow is more deflected and the length ratio a/b is greater. The result is that a turbine stage can be operated with a greater ratio a/b, hence with a greater spacing ratio a/t or with a greater deflection of flow, than a blower stage.

The present estimate gives obviously only an approximate picture of the separation danger since the effect of blade form[1] and profile chord, for example, are not mentioned at all. But even so it serves as a guide for the evaluation of grids of highly cambered blades, for which there are practically no test data available.

The preparation of more accurate data on profile form is the purpose of the present report. The maximum lift coefficient $c_{a\ max}$ is not suitable for evaluating the separation danger on highly curved blades in cascade arrangement, because existing constant pressure turbines operate at lift values[2] up to 6, while the flow over an airplane wing already separates at $c_{a\ max} \sim 1.5$.

On the airplane wing there exists a definite relationship between lift coefficient c_a and the parameter $\frac{p_2 - p_3}{q}$ introduced here. On

---

*Reviewer's note: This equation does not agree with Figure 3B. In order to do so, $\frac{p_2 - p_3}{q}$ should be changed to $\frac{p_1 - p_3}{q}$.

[1]That closely spaced, highly curved blades, for which the flow is very considerably dependent upon the blade form, can result in a pressure distribution other than triangular is shown in figure 9.

[2]The relation for blade grids is $c_a = \frac{a}{t} 2\left(\frac{w_{u2} - w_{u1}}{w_\infty}\right)$ where w_∞ is the value of the vectorial mean of the two velocities w_1 and w_2.

substituting a triangle for the pressure distribution plotted against the profile chord t, the lift A per unit of span is $A = \Delta p_m \frac{t}{2}$, while, by definition, $A = c_a \, tq$. Lastly:

$$*p_2 - p_3 = \Delta p_m - q; \text{ hence } \frac{p_2 - p_3}{q} = 2c_a - 1.$$

The parameter $\dfrac{p_2 - p_3}{q} \sim 2$ is therefore equivalent to the maximum lift coefficient of wings $c_a \sim 1.5$.

III. THE INTERFERENCE METHOD

The tests were made with a Mach-Zehnder interferometer (reference 6) manufactured by Zeiss, (fig. 4). It consists essentially of four plane mirrors, two of them $\left(a_1 \text{ and } a_2\right)$ being "half-silvered," and the other two $\left(b_1 \text{ and } b_2\right)$ with opaque silver coating. Every beam of light from the light source c, is split into two parts at the half-silvered plate a_1, and reaches the screen e by different paths. One part is reflected at a_1, reaches mirror b_2, passes through mirror a_2 and reaches screen e with a portion of its intensity. The beam going through mirror a_1 arrives after reflection at the mirrors b_1 and a_2 at the screen e. The two light rays passing through the interferometer when superimposed produce interference fringes at the point of intersection (reference 1). If the four mirrors are perfectly parallel the two light rays leaving plate a_2 intersect at infinity. Thus the interference fringes would occur at infinity. Since the wave fronts of the two light rays are parallel to each other, however, the width of the interference bands is infinitely great. Bands of finite width at infinity are obtained when the two mirrors a_1 and a_2 are turned through a small angle α_1 and α_2 out of their neutral position. The plane in which the interference bands originate can be shifted to any position at infinity and the width itself can be adjusted as desired by corresponding choice of angle α_1 and α_2. At the setting of the mirrors shown in figure 4, the two light rays move in divergent directions from plate a_2. Their extension backward meets in the plane 1 - 2, however, so in this plane a virtual interference pattern is produced. This picture can be made visible on screen e by a converging lens d and photographed. In reality, a more complicated optical device takes the place of the lens. For the subsequent application of the interferometer the plane 1 - 2 must be placed in the position between mirrors a_2 and a_1

---

*Reviewer's note: This equation is correct only if q is changed to q_2. If that is done the lift coefficient c_a is based on q_2 which is unusual but not necessarily incorrect.

shown in figure 4. If the axes of rotation of mirrors a_1 and a_2 are normal to the plane of the drawing, the interference fringes thrown on the screen are parallel to the axes of rotation. By swinging mirror a_2 about a second axis which lies in the mirror plane and is normal to the first axis, the direction of the bands can be varied at will. Their relative spacing is varied by the adjustment of the angles α_1 and α_2. Monochromatic light produces contrasting interference fringes in a larger field. For the present purpose a mercury vapor lamp with a monochromatic filter which lets through light of the wavelength $\lambda_\infty = 0.5641 \times 10^{-3}$ millimeter was employed.

Placing a chamber f closed by two flat parallel windows g and filled with a gas in the path of the rays and varying the density ρ of the gas in the chamber by a value ρ', the interference pattern shows a shift of the bands. The density variation in the chamber $\Delta\rho = \rho' - \rho$ can be computed from the observed band shift by the formula (reference 1)

$$\Delta\rho = \frac{\rho \lambda_o \epsilon}{L(n-1)} \tag{11}$$

λ_o is the wavelength of the light in vacuum, ϵ the band shift measured in widths (one width equals the distance of the center lines of two successive light and dark bands), n the index of refraction of the gas of density, ρ and L the path-length of the light rays in the medium of density ρ'. The expression $\frac{n-1}{\rho}$ has a constant value for every gas. For air $\frac{n-1}{\rho} = 0.002265 \frac{m^4}{kg\ s^2}$. The path length L for the setup used is given by the inside distance between the two windows g. It amounts to 199.8 millimeters. These values entered in equation (11) give

$$\Delta\rho = 0.001246\,\epsilon\,\frac{kg\ s^2}{m^4} \tag{12}$$

Given the type of change of state by which the density variation $\rho' - \rho$ of the gas in the chamber f was obtained, all the other conditions of state can be computed from the fringe displacement. For the isentropic change of state of an ideal gas it is $p'/p = (\rho'/\rho)^\kappa$ and $T'/T = (\rho'/\rho)^{\kappa-1}$, for example. Through the density ρ' computed by equation (11) the

pressure p' and the temperature T' are defined. Likewise, for an
isobaric change of state the gas equation $\frac{p}{\rho} = RT$ gives the
temperature $T' = T\left(\frac{\rho}{\rho'}\right)$.

In place of chamber f the test section of a flow channel closed
at both sides by parallel windows g is placed in the path of the rays.
The blades to be studied are fitted into this channel in such a way that
the light rays pass parallel to the generating axis of the blades.
Through the air flow a density field is formed around the blades. Now
the density has a different value for the path of each light ray through
the channel. The result is a distortion of the interference fringes.

The blade grid, itself, together with the interference fringes
originating in the plane 1 - 2, is reflected on the screen e. Therefore,
the density field around the blades can be determined by measuring the
deflections of the interference fringes at each point of the screen. As
is seen from the subsequent photographs the density field of the flowing
air made thus visible brings out the extent of the boundary layer as well
as its separation.

IV. EXPERIMENTAL LAYOUT

The flow channel into which the blade grid was mounted is shown in
two sections in figure 5, and in photograph figure 6. The air is induced
by a blower through the rectangular inlet cone a and flows past the
blading b. The air jet leaving the screen is intercepted by the exit
cone c and returned to the blower by way of the diffuser d and a
pipe line connected by a flexible leather collar. The blower is driven
by a direct-current motor so that its speed can be controlled within wide
limits. It produces a maximum pressure difference of 260 millimeters of
water. Since the flow through the blades was to be explored at different
flow angles, the front - and back wall f of the air channel before the
blading are pivotable about the two rotational axes g. The blade grid
could be investigated for six flow directions. Every setting called for
a different entrance cone a. The two parallel windows i were mounted
in the heavy side walls h of the channel. The front - and back wall f
was sealed from the sides h by rubber collars and plasticine. The
blades b are suspended from two tension wires k of 2 millimeter gage
and sealed from the glass windows by glued on rubber washers l. To
prevent the exit direction of the air flow from the blading from being
influenced by the position of the exit cone c, the dead air regions m
and n existing at either side of the jet were joined by two strong pipe
lines, by which a pressure balance is maintained between the dead air
regions. In spite of this the uniformity of the air jet behind the blade
grid is so far still not quite satisfactory, and is to be improved on the
newly designed set-up by larger dead air regions m and n. The blades

were impregnated beech wood. Great care was taken to ensure the best possible two-dimensional blade form, (flat, parallel generating line), because the light rays must pass parallel to the blade as exactly as possible over its entire length if an observation of the flow processes in the thin boundary layer of the blade surface is to be possible. Appropriate gages ensure exact parallel setting of the blades during assembly on the tension wires. The grid spacing was varied by changing the number of blades. The surfaces were finished with shellac to ensure smoothness. In figure 7 two blades together with the tension wires are reproduced. In the majority of the tests described hereinafter the middle blade of the screen was heated. To this end the blade was provided with two holes o into which a chromium-nickel heating coil on a ceramic tube was inserted. Owing to the low thermal conductivity of the wood it was, of course, not to be expected that the blade surface would reach a constant temperature, which, however, did not matter in the present tests. The exact alinement in the light rays of the interferometer was obtained by means of three set screws p. From the 146 millimeter diameter circle presented by the window for inspection, the interferometer covers a rectangular field of view of 8×10 centimeters. The position of the field can be changed by shifting the test section.

The flow velocity w_0 of the blades is computed from the negative pressure $\triangle p$ measured at the orifice r relative to the test room, by the equation

$$\triangle p = \lambda \, \frac{w_0^2}{2g} \tag{13}$$

λ = density of air. The upper wall f of the channel contains further three orifices s closed by threaded plugs, into which a small pitot tube can be inserted, for checking the uniformity of air flow in front of the blades. Up to a thin boundary layer at the side walls the velocity over the cross section was practically constant and agreed with the figure obtained by equation (13) to a few tenths of one percent. A check of the flow behind the blades by pitot tube is afforded by a flange, shown in figure 5, replacing one of the two glass windows. The flange consists of a ring t and a concentric disk u which can be turned by means of a handle v. Its setting is read from a scale w. This disk carries a hole x for inserting a pitot tube. By moving the pitot tube in this orifice and turning the disk u the flow in the section behind the blades can be measured. This is important, in order to ascertain whether the flow separates from the side walls h. This phenomenon was repeatedly observed on blower blade grids (references 5 and 7). It is also intended to use this method to measure the wake defect behind the blades, and thus to establish the blade drag and the energy loss of the air at passage through the grid.

V. EXPERIMENTAL RESULTS

A section of flow photographs for different spacing ratios and flow angles is represented in figures 8 and 10 to 30. The shape of the blades tested, visible from the pictures, was suggested from other tests. The blade exit angle, measured between the bisectrix of the blade trailing edge and the cascade direction, is 15° for these blades. Aside from the two end pieces, which at the side facing the inside of the channel, were shaped to conform to the blade profile, figure 5, two to four blades were mounted in the working section. This made spacing ratios a/t, (fig. 2), of 0.687, 0.859, and 1.141 possible. The chord of the blade profile is 58.2 millimeters. It was measured, as for a wing, as projection of the blade profile on a straight line touching the lower surface of the blade, figure 1. Through the different settings of the channel walls f and the related entrance cones flow angles of 20, 34, 48, 62, 76, and 90° were obtained.

Figure 8 shows an interference photograph at 0.687 spacing and 34° flow angle. The deflection of the interference fringes caused by the density field in the flowing air is plainly visible. Directly at the blade surface the interference lines have a bend, that is, an especially great density gradient exists at the surface[3], which is due to the fact that the boundary layer of the flow is heated as a result of the heat (heat of dissipation) liberated by internal friction. This phenomenon makes it possible, as already indicated by Th. Zobel, to render the boundary layer visible by interference photographs. Even the dead air region behind the blade trailing edge, which is formed by the warmer air in the boundary layer, is clearly shown. Outside of the boundary layer and the dead-air region the air flow is, of course, free from loss, the change of state of the air in this area is therefore isentropic, hence the pressure field within the flow can be computed from the density field defined by the interference photographs by means of the previously cited relations. This method also yields the pressure distribution along the blade surface from the fringe displacements at the border of the boundary layer, as exemplified by the pressure area, figure 9, where the pressure distribution is plotted against the grid width b (fig. 2), hence against the blade projection on a normal to the grid direction. The area of the pressure surface indicates the tangential force acting on the blade. The photograph, figure 8, was made at 21.7 meters per second air speed. The mean exit velocity at the end of the blade channel computed from the continuity equation was 89.5 meters per second. The mean velocity at the same point from the interference record is 91.6 meters per second. The blower operated at its maximum speed. The fringe movements (fig. 8) are not yet very great at these velocities, and the accuracy with which the tangential force on the blade can be determined from the interference photographs is, as a result, not quite satisfactory. This drawback is easily removed by addition of a stronger blower. The boundary layers at the blade inlet side where the velocities are comparatively low, are not clearly visible in figure 8.

---

[3]Unfortunately, many details on the photographs are not as clear as on the originals.

Since for the study in question, however, it is important to observe the separation of the boundary layer, even at the low velocities, the temperature of the boundary layer was raised artificially by heating the blade. According to the Navier-Stokes differential equations for frictional fluid flow the field of flow is not affected by temperature differences if the fluid properties (density, viscosity) are not dependent upon the temperature and the lifting forces in the flow introduced by the temperature differences disappear with respect to the inertia forces. And this is certainly the case at the speeds and low increases of temperature of 25° at the most produced within the boundary layer by the heating[4]. Figures 10 to 30 represent interference photographs with such blade heating. The two heavy parallel lines are the shadows of the current supply wires, carried in thin insulating tubing along the upright side walls of the entrance cone, figure 6. The flow direction is nearly the same as the direction of these wires.

Figures 10 to 15 show the flow at the smallest spacing ratio $a/t = 0.687$, figures 16 to 21 at $a/t = 0.859$, and figures 22 to 27 at the greatest spacing ratio $a/t = 1.141$. Reverting to figures 10 to 15 it is seen that for this smallest flow angle the flow already breaks down near the stagnation point on the back of the blade. According to figure 10 the interference fringes at a certain distance from the blade's surface disappear completely after a bend. That the area actually indicates the dead air behind a separation zone is plainly seen in figure 27. The bend of the interference fringes at the back of the blade somewhat downstream from the support wire breaks away from the surface of the blade. This indicates the surface of discontinuity which always emanates from an area of separation of flow. Such a surface of discontinuity dissolves in vortices. This is manifested in the washed out fringes as soon as the vortex frequency is sufficiently great. This is particularly plain from the separation at the face of the blade of figure 27. Larger vortices of correspondingly lower frequency are no longer seen in the photograph; but they can be observed on the ground-glass plate by oscillation of the interference fringes in the dead-air regions. The disappearance of the interference lines inside a narrow strip along the face of the blade in figure 10 is probably due to the deflected interference fringes being extremely thin at this point and not reproduced on the photograph. The

---

[4]Figures 10 to 30 indicate that the interference fringes in the boundary layer have a maximum deflection of eight interference fringe widths. Thus the maximum density difference in the boundary layer between blade wall and free flow is, by equation (12), $\Delta\rho = 0.00997 \dfrac{\text{kg s}^2}{\text{m}^4}$. The air density in the tests was about $\rho = 0.12 \dfrac{\text{kg s}^2}{\text{m}^4}$. Since the change of state in the boundary layer can be regarded as isobaric, we get $\dfrac{\Delta T}{T} = -\dfrac{\Delta\rho}{\rho}$, as it follows immediately from the equation of state for a small change of state. Therefore the maximum temperature difference inside the boundary layer is $\Delta T = 24^{\circ}$. The displacement by eight widths, however, occurs only in very isolated cases. On the average it, and hence the temperature differences inside the boundary layer, are substantially less.

dead-air zone at the back of the blade disappears again downstream. It is
readily seen how, starting from the suspension wire, a new boundary layer
is formed in the accelerated flow. At the next greater flow angle,
figure 11, however, the separation at the back of the blade has already
disappeared. But at the great angles of setting, figures 14 and 15, the
flow breaks down at the front side in the vicinity of the stagnation
point. The flow adheres again farther downstream. In figure 13 a slight
breakaway is probably under way.

The same phenomena recur for greater spacing ratios. At $a/t = 0.859$,
figures 16 to 21, a second region of separation is observed, at the back
of the blade downstream from the end of the blade passage. In figure 16
this second breakdown is not quite so conspicuous. A variation of the
interference fringe right next to the blade surface is noticed at the
same place as in the subsequent photographs. Behind this region the flow
remains separated. The result is an expansion of the wake behind the
blade trailing edge. The exiting velocity direction, as shown by the
direction of the wake, is no longer exactly the same as the direction of
the blade trailing edge. The blade grid is, at this spacing, no longer
capable of completely deflecting the flow as far as the blade exit angle.

The separation phenomena at $a/t = 1.141$, figures 22 to 27, are
very pronounced. The wake behind the blades is very wide, as evidenced
from the direction of the discontinuity surfaces arising from the regions
of separation, and the direction of the outgoing flow is far from the
blade exit angle. The blading is impractical for a turbine at this
extremely large spacing ratio.

According to the photographs the blading can be used up to $a/t = 0.859$
and at flow angles ranging between 34 and 62°. The slight separation on
the back of the blade at $a/t = 0.859$ should not cause perceptible impair-
ment of the efficiency, since the width ratio of the wake given by the
rounding of the blade trailing edge to the width of the undisturbed air
stream at the blade exit decreases with increasing spacing ratio. A
sharp exit edge would reduce the width of the wake, so that the flow condi-
tions would certainly be improved through the grid.

Since there is a possibility that the separation phenomena at the
blades are affected by the Reynolds number, the blading was investigated
with $a/t = 0.859$ at various flow velocities. Three photographs from this
test series are represented in figures 28 to 30. It is seen that the
separation is diminished at the higher speeds. If the Reynolds number is
calculated using the axial component, $\overset{\cdot}{w}_m$, of the flow velocity and the
blade chord t, its magnitude for figure 28 is 11800, for figure 29,
22300 and for figure 30, 35400. The axial component was used for calcu-
lating the Reynolds number because it can be precisely calculated on the
actual turbine from the discharge volume and the flow cross sections. Gas
or steam turbines operate with blades of from 1 to 3 centimeters chord and
flow velocities in axial direction w_m of from 100 to 300 meters per second

The gas - or vapor - temperatures range between 1000 and 200 degrees and the pressures between 10 and 1 atmosphere, except for maximum pressure turbines. This gives a Reynolds number ranging between 10^3 and 10^6. In consequence the present test range lies approximately midway in the practical range. One condition for the applicability of these data is, of course, that the Mach number does not exceed the value 0.6 to 0.7, which usually is the case on gas turbines.

VI. SUMMARY AND OUTLOOK

To provide basic data for the design of turbine blading the flow through a blade grid of highly curved profiles was analyzed by the interference method. The density of the air passing through the grid was determined from the records and the pressure distribution past the blades and the force produced by the pressures on the blade were obtained. Since the boundary layer of the flow at the blade surface is plainly visible on the interference records, any separation of flow is readily recognized. These separation phenomena were studied first. It is expedient to use comparatively large model blades in the tests. Limiting the Reynolds numbers to values usual for turbine operation, therefore, gives proportionally low airspeeds. One of the blades was slightly heated in order to make the boundary layer visible at these speeds also.

The flow through a turbine blade grid with good (advantageous) blade profiles was examined at different spacing ratios and flow angles. The interference photographs of the flow through this grid as represented in figures 10 to 27 indicate that at the smallest flow angle (20°) the flow has already separated from the back surface of the blade just behind the inlet stagnation point. The flow separates likewise on the face of the blade at great flow angles (60° to 90°). In both cases, however, the flow follows the blade closely again when the spacing ratio is small. At greater ratio (say from $a/t = 0.859$ on), separation occurs again at the back of the blade near the trailing edge. Behind this region of separation, however, the flow no longer follows the blade surface. Thus the separation leads to expansion of the wake behind the blade and so certainly to a substantial impairment in efficiency. The described separation phenomena are affected by the Reynolds number, as was determined in a special test series (figs. 28 to 30).

The tests are at present being extended to other blade forms, with the aim of developing suitable blade forms that ensure separation-free flow within a wide range of flow angles and spacing ratios. The tests are also to be extended to include blower blades. The flow losses can be determined by momentum measurements in the wakes behind the blades and the efficiency of the blading defined numerically. Since the temperature conditions in the boundary layer on the blade surface can be determined from the interference photographs, this method is particularly suitable

for the study of the efficiency of the different methods for blade cooling.
The effect of the Mach number on the flow is to be investigated also.

Translation by J. Vanier,
National Advisory Committee
for Aeronautics.

REFERENCES

1. Schardin, H.: Z. Instrumentenkde. Bd. 53, 1933, pp. 396-403
      and pp. 424-436.

2. Zobel, Th.: Z. VDI, Bd. 81, 1937, pp. 619-624.

3. Weinig, F.: Die Strömung um die Schaufeln von Turbomaschinen.
      (Leipzig), 1935, pp. 125-137.

4. Ergebnisse der aerodynamischen Versuchsanstalt, Göttingen,
      III. Lieferung, 1935, pp. 132-137.

5. Christiani, K.: Luftfahrtforschung Bd. 2, 1928, pp. 91-100.

6. Hansen, G.: Z. techn. Physik. Bd. 12, 1931, pp. 436-440.

7. Keller, C.: Axialgebläse vom Standpunkt der Tragflügeltheorie.
      Mitteilg. a.d. Inst. f. Aerodynamik. ETH (Zürich) 1934.
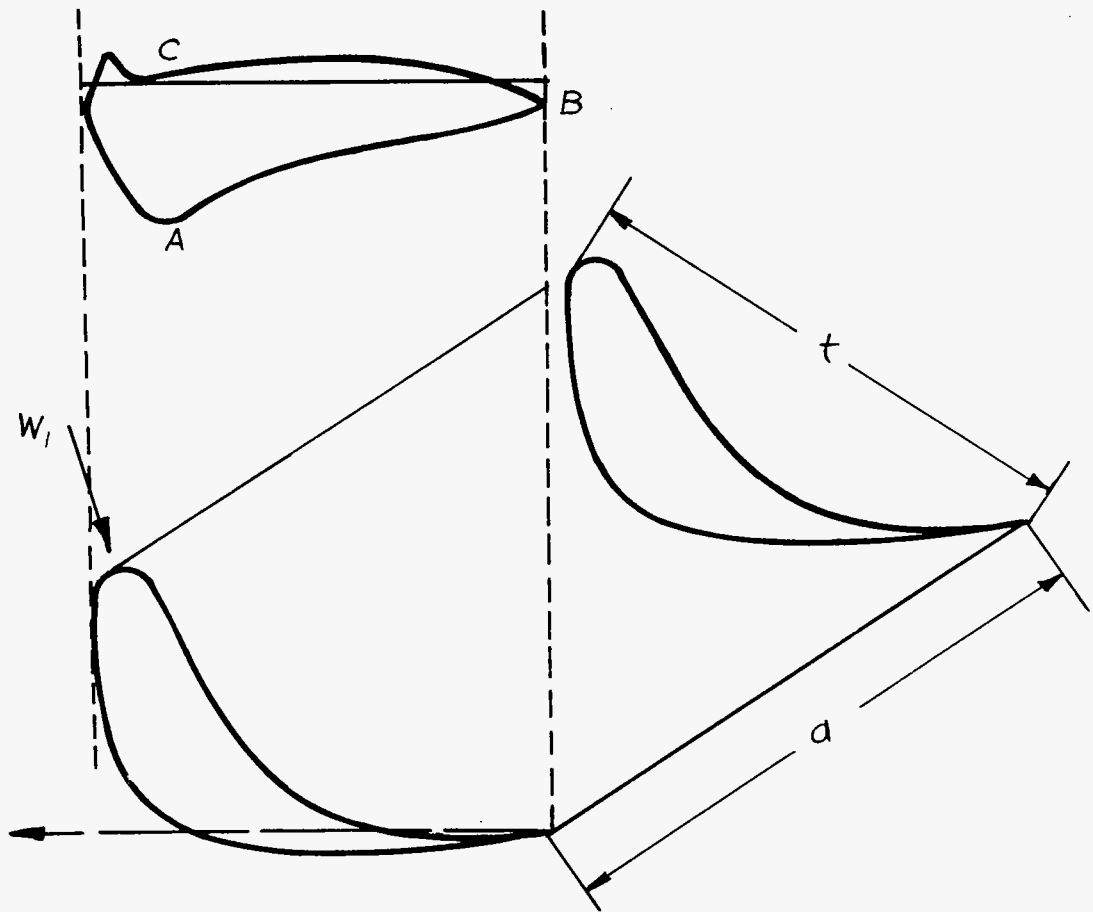
Figure 1.- Pressure distribution around a turbine blade (Weinig).
t = blade chord, a = spacing, w_1 = flow velocity.
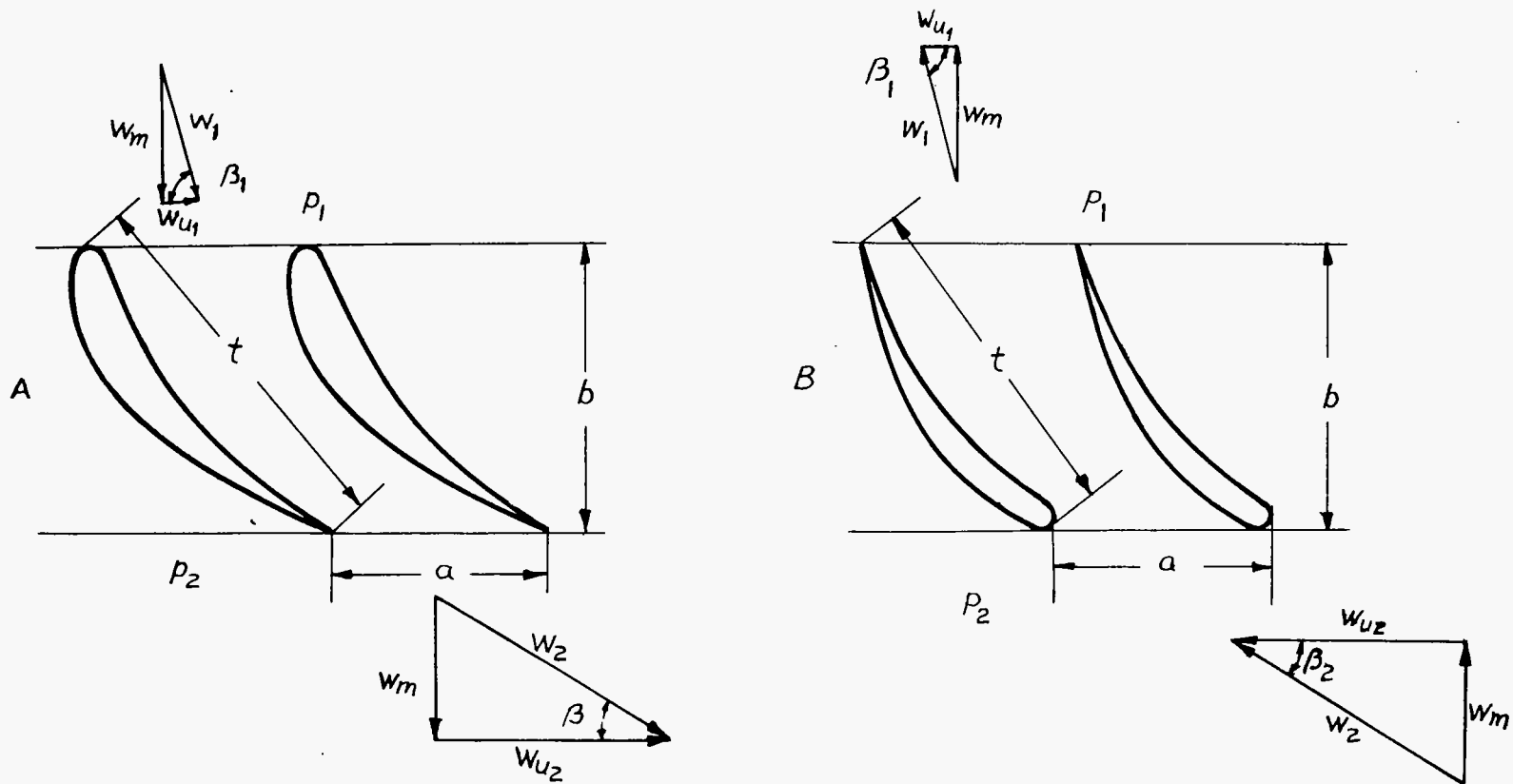
Figure 2.- Blade grid.

A	turbine blades	w	velocity
B	blower blades	w_m	axial component of the velocity
t	blade chord		
a	grid spacing	w_u	circumferential component of the velocity
b	grid width		
$\frac{a}{t}$	spacing ratio	β	entrance and exit flow angle
p	static pressure		
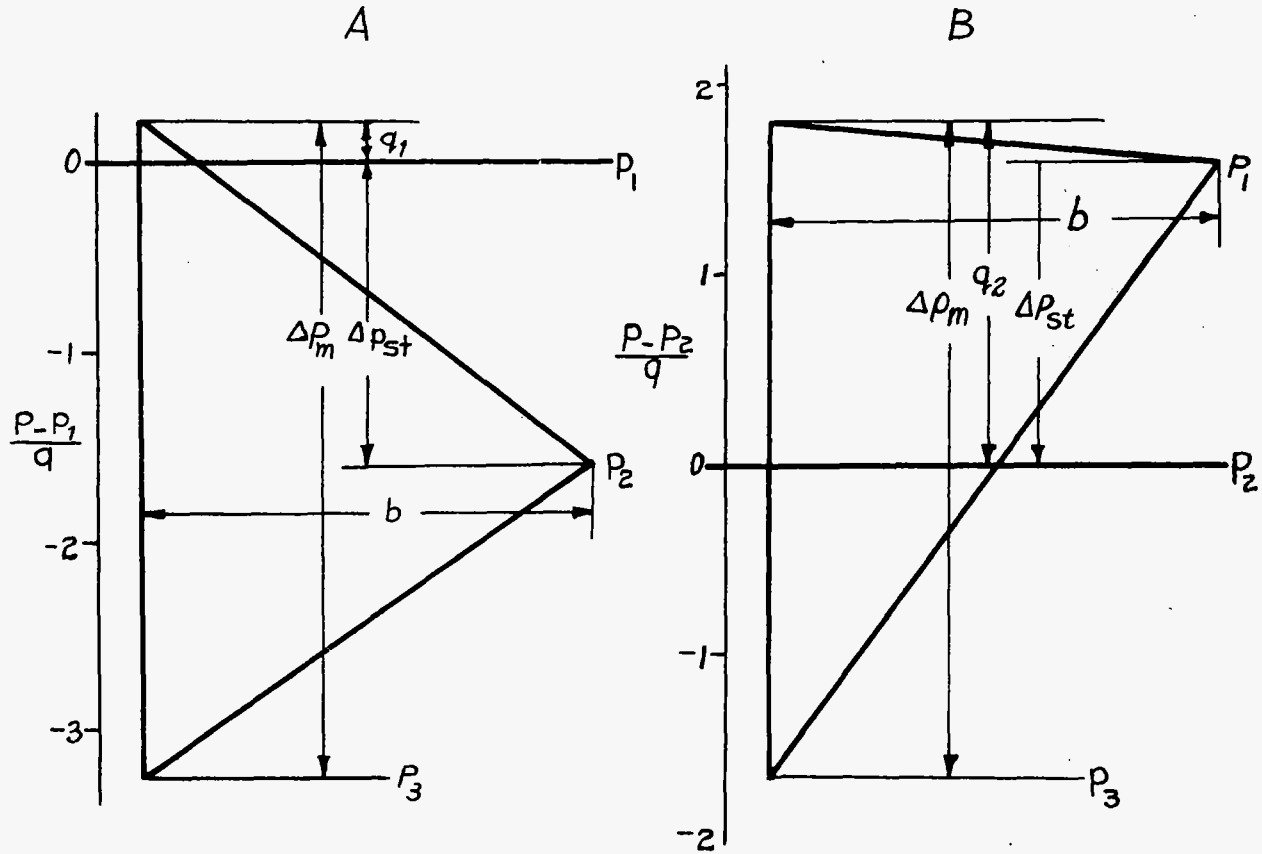
Figure 3.- Approximate pressure distribution past a turbine blade A
and a blower blade B.

b	width of grid	Δp_m	maximum pressure difference
p	static pressure		
q	dynamic pressure	Δp_{st}	pressure change of the stage
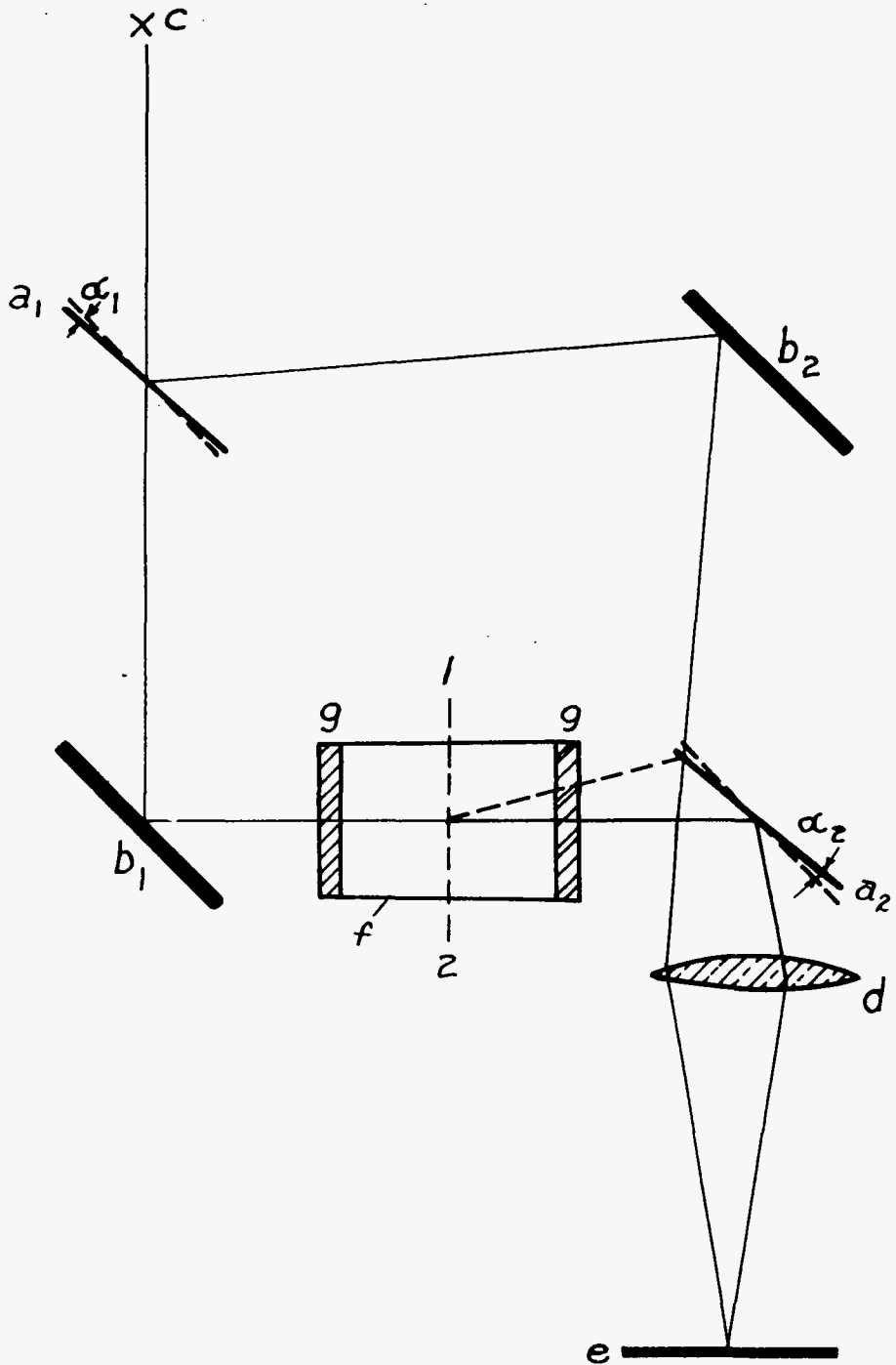
Figure 4.- Plan of the Mach-Zehnder interferometer.

a	half-silvered mirrors	e	screen
b	full-silvered mirror	f	chamber
c	light source	g	parallel glass windows
d	lens	α	angle of inclination

┤ A

Section C-D

Section A-B
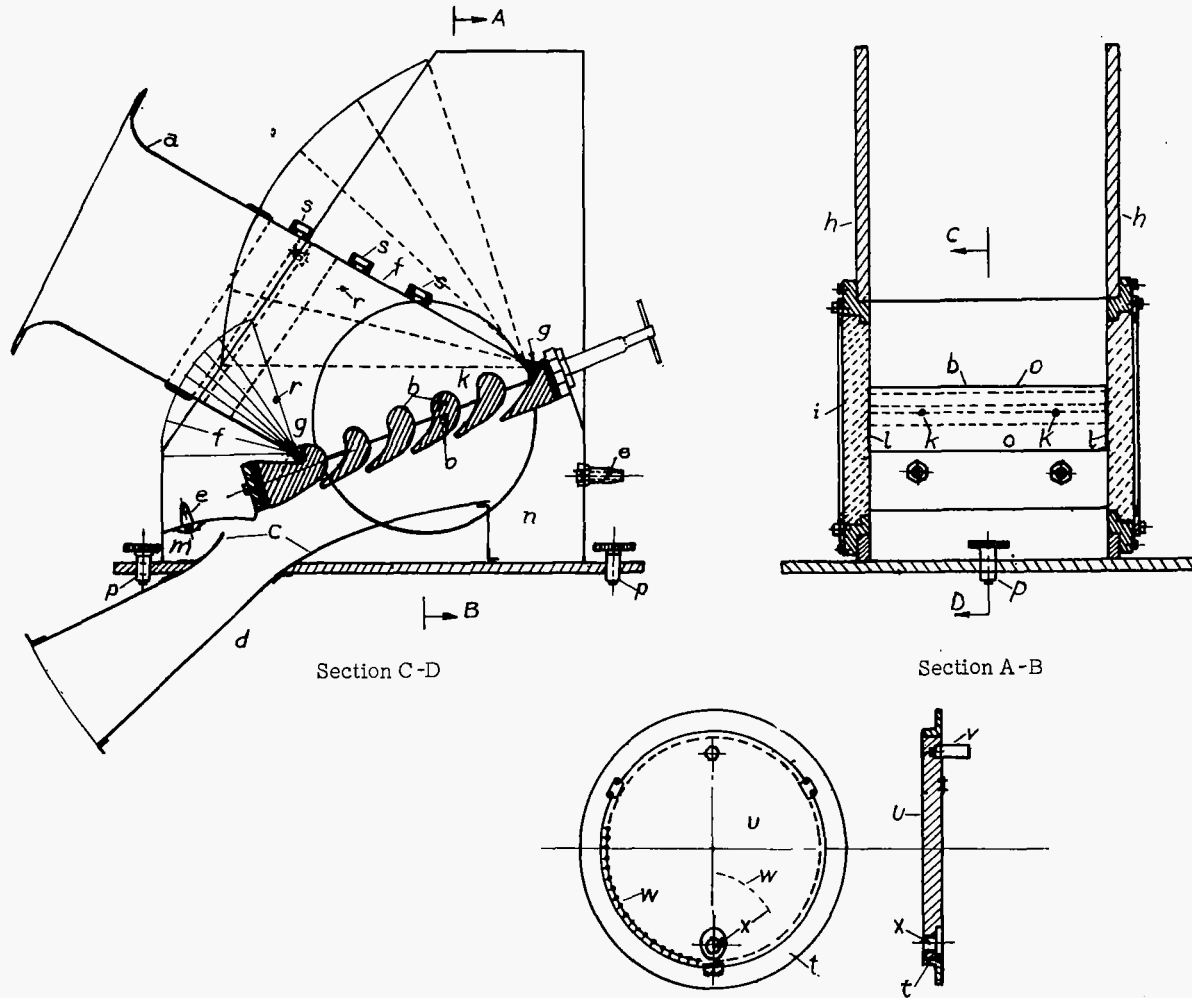
Figure 5.- Experimental setup.

a	entrance cone	g	rotational axes of walls f	r	pressure taps
b	blade grid	h	side walls	s	orifices for pitot tube insertion
c	exit cone	i	parallel glass window	t	ring
d	diffuser	k	tension wires	u	plate
e	nipple for pressure equalizing lines	l	rubber washers	v	handle
f	front and back wall of entrance channel	m,n	dead-air regions	w	scale
		o	holes	x	orifice for inserting pitot tube
		p	set screws		

Page intentionally left blank
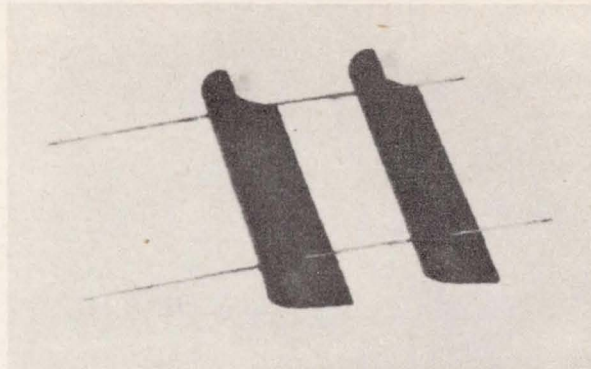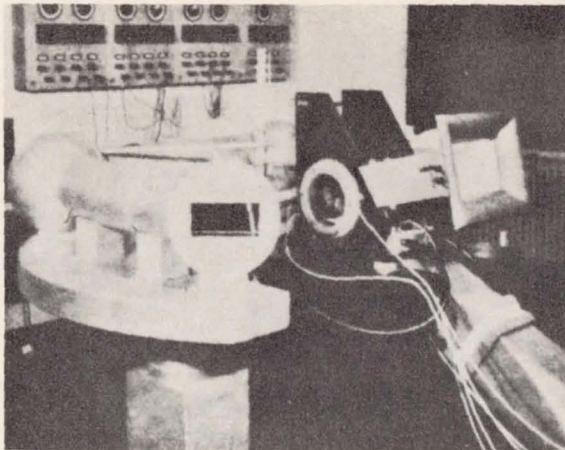
Figure 6.- Interferometer with test setup.   Figure 7.-   Blades with tension wires.
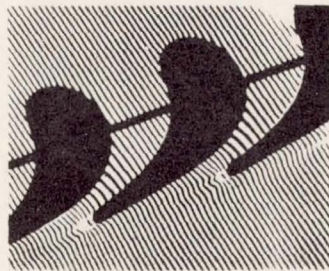
Figure 8.- Interference photograph for predicting the pressure distribution around a turbine blade.

Spacing ratio $\frac{a}{t}$ = 0.687

Flow angle β_1 = 34°

Reynolds number $R = \frac{w_m t}{\nu}$ = 53,000

Page intentionally left blank
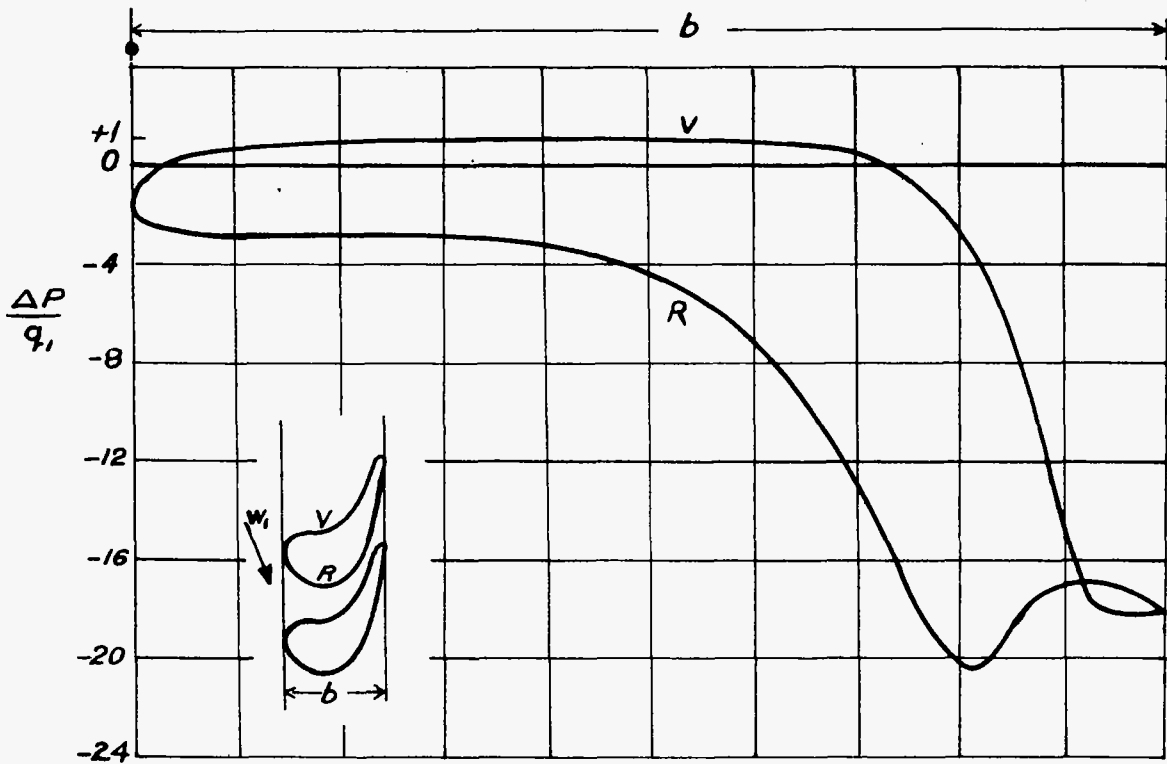
Figure 9.- Pressure distribution around a turbine blade according to figure 8.

b   width of blade grid
Δp difference between local pressure and static pressure of flow
q_1 dynamic pressure of flow
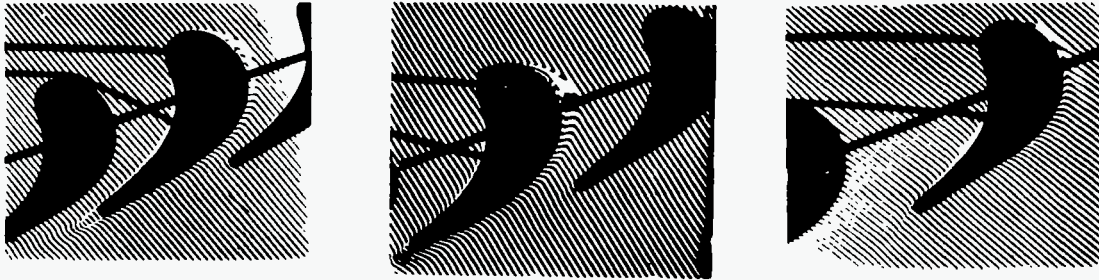
Figure 10, 16, 22: $\beta_1 = 20^O$

Figure 11, 17, 23: $\beta_1 = 34^O$
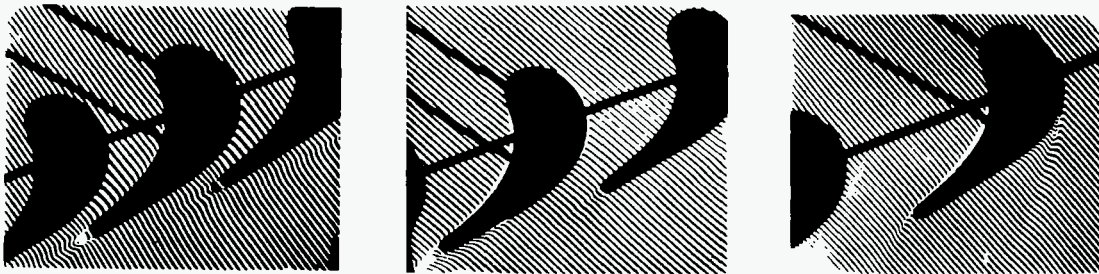
Figure 12, 18, 24: $\beta_1 = 48^O$

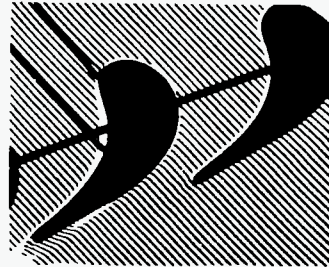Figures 10-27.- Interference photographs of flow around a turbine blade grid with different spacing ratios (a/t) and flow angles (β_1).
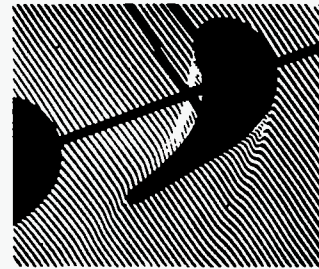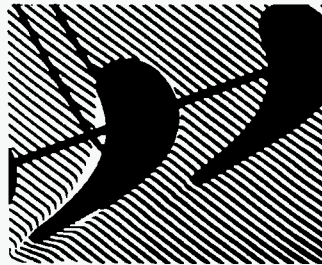
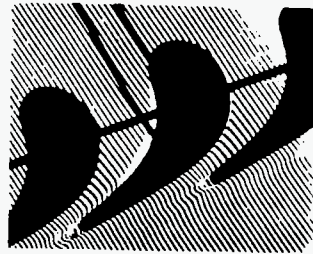Figure 13, 19, 25: $\beta_1 = 62^{\circ}$

Figure 14, 20, 26: $\beta_1 = 76^{\circ}$

Figure 10 to 15: $\dfrac{a}{t} = 0.687$ Figure 15, 21, 27: $\beta_1 = 90^{\circ}$ Figure 22 to 27: $\dfrac{a}{t} = 1.141$

Figure 16 to 21: $\dfrac{a}{t} = 0.859$

The flow direction is about the same as that of the two dark parallel shadows. The Reynolds number for figures 10, 16, 17 lies between 16,000 and 20,000, for the others between 42,000 and 54,000.

Figure 28:   Re = $\dfrac{w_m t}{\nu}$ = 11,800 Figure 29:   Re = $\dfrac{w_m t}{\nu}$ = 22,300 Figure 30:   Re = $\dfrac{w_m t}{\nu}$ = 35,400

Figure 28-30.-   Interference photographs of flow through a turbine blade
grid at different Reynolds numbers (R).

w_m, axial component of the velocity; t, blade chord; ν, kinematic viscosity;
$\dfrac{a}{t}$ = 0.859, spacing ratio; β_1 = 34°, flow angle.